Journal of Thermal Analysis and Calorimetry (2022) 147:753–762
https://doi.org/10.1007/s10973-020-10313-w

Thermal performance analysis of a low volume fraction Al_2O_3 and deionized water nanofluid on solar parabolic trough collector

G. Vijayan[1] · P. P. Shantharaman[2] · Ramalingam Senthil[3] · R. Karunakaran[4]

Received: 25 February 2020 / Accepted: 26 September 2020 / Published online: 13 October 2020

Abstract
The present work analyzes the performance of unshielded receiver tube integrated solar parabolic trough collector where Al_2O_3/deionized (DI) water nanofluid of low concentrations was used as heat transfer fluid (HTF) element. Nanofluid is synthesized at various volume fractions starting from 0.2 to 1.0% with surfactant-free condition, by ultrasonic technique. Several researchers investigated the performance of higher nanofluid concentrations (1.0–5.0%) with and without surfactants on parabolic trough solar collector. The outdoor experiments are conducted for two HTF flow rates of 0.010 kg s^{-1} and 0.015 kg s^{-1}. When the nanofluid is subjected as HTF, the DI water acted as a base fluid. While DI water is allowed to flow through the absorber, it performs both as HTF and heat storage fluid. The synthesized nanofluid at various volume fractions is allowed to flow through the receiver for the purpose of analyzing the thermal performance and compare the results with DI water. The collector efficiency increases with the mass flow rate as well as the concentration of nanofluid. For 0.015 kg s^{-1}, the maximum efficiency was calculated as 59.13% (hourly) and 58.68% (average).

Keywords Alumina nanofluid · Deionized water · Concentration · Solar parabolic trough collector · Unshielded receiver

List of symbols

A	Area (m^2)
CR	Concentration ratio (–)
DI	Deionized (–)
D	Diameter (–)
F, R	Factor (–)
HTF	Heat transfer fluid (–)
I	Radiation (W m^{-2})
K	Thermal conductivity (W m^{-1} K^{-1})
$K(\theta)$	Incident angle modifier
L	Aperture length (m)
m	Mass (g)
Nu	Nusselt number (–)
Pr	Prandtl number (–)
Q	Heat gain (W)
Re	Reynolds number (–)
S	Solar flux (W m^{-2})
SPTC	Solar parabolic trough collector (–)
T	Temperature (°C)
U, h	Coefficient (W m^{-2} K^{-1})
USR	Unshielded receiver (–)
V	Volume (m^3)
W	Aperture width (m)

Subscripts

a	Aperture, ambient
b	Beam, tilt
bf	Base fluid
fi	Nanofluid inlet, inside heat transfer
fo	Nanofluid outlet
i	Inner
ins	Instantaneous
l	Heat loss
np	Nanoparticle
opt	Optical
r	Radiation loss
R	Heat removal

✉ G. Vijayan
viji_laker@yahoo.co.in

[1] Department of Mechanical Engineering, KSK College of Engineering and Technology, Anna University, Kumbakonam, Tamil Nadu, India

[2] Department of Mechanical Engineering, Kings College of Engineering, Anna University, Punalkulam, Tamil Nadu, India

[3] Department of Mechanical Engineering, SRM Institute of Science and Technology, Kattankulathur, Chennai, India

[4] Department of Mechanical Engineering, University College of Engineering-Tirukkuvalai, Anna University, Chennai, India

Greek symbols

Ω	Hour angle
ϕ	Volume fraction
η	Efficiency
$\dot{\rho}$	Reflectivity
u	Useful
w	Wind loss
θ	Incident angle
τ	Transmittance
α	Absorptance
Υ	Intercept factor
σ	Stefan–Boltzmann constant
εr	Emissivity

Introduction

Depletion of fossil fuels, the release of enormous amounts of greenhouse gases, and subsequent global warming are the pendulum points for both the scientists and researchers, to focus on renewable sources of energy like solar energy, wind energy, ocean energy, and geothermal energy, which are clean, evergreen, and available abundantly. Even though many renewable sources of energy are available, solar energy is the most promising one, to utilize in an easy way with a low cost. For most of the thermal applications, it is required to generate the energy at a higher level than that of the flat plate solar collectors. The concentrated solar collectors like parabolic trough or dish types are used to attain a higher energy level. Maximum heat energy is achieved by decreasing the absorber area which will decrease the heat loss and increase the useful heat gain at a higher concentration ratio. Solar energy is widely used for hot water, industrial process heat, steam generation and electricity production [1]. Encapsulated phase material-based thermal energy storage system for concentrating solar power plant was analyzed for uninterrupted operation as well as to ensure the techno-economic status of storage material [2]. Sheikholeslami et al. [3] designed clean energy storage unit to reduce the energy consumption through civil structural instead of increasing the space between air passage and phase change material. Curing process completed 21.4% faster than other case, which ensured the system validation. Conical geometry solar collector was designed and tested for its thermal performance for producing hot water where deionized water-based alumina nanofluid as heat transfer medium [4]. The solar parabolic trough collector (SPTC) is the most mature technique for steam production where different types of nanofluid with various concentrations used. Vijayan and Karunakaran [5] investigated the performance of unshielded receiver type SPTC, where water as HTF. They observed the maximum difference in temperature as 24 °C. The mixed type storage tank integrated SPTC model was developed using MATLAB software. The model is experimentally verified and analyzed for its performance. The enhancement of maximum temperature difference between analytical and experimental storage tank was observed as 9.59% [6]. Valanarasu and Sornakumar [7] carried out the experimental work on SPTC and recorded the temperature difference of 38.84º, during the test time period of 9.30–4.00 pm, where no heat energy was removed. Bellos et al. [8] experimentally analyzed various HTFs such as pressurized water, molten nitrate salt, carbon dioxide, air, sodium liquid, and helium on SPTC for higher temperature range. Bellos et al. [9] investigated the performance of various Syltherm 800-based nanofluids (Cu, CuO, Fe_2O_3, TiO_2, Al_2O_3, and SiO_2) on SPTC and observed Cu as an efficient one among various types of nanofluids, where the fluid flow rates vary from 50 to 300 L min^{-1}. The thermal efficiency enhancement of Cu nanofluid was 0.74% at 6.0% concentration. The latest developments in solar concentrator and performance enhancement methods such as nanofluid, turbulator, insert, and absorber geometry modification are discussed [10]. The deionized (DI) water and ethylene glycol-based aluminum oxide nanofluid were synthesized using magnetic stirrer cum ultrasonication, and thermal properties were analyzed [11]. Murshed et al. [12] analyzed the variation, trend, and influence of temperature on thermophysical properties such as thermal conductivity, specific heat and viscosity.

Sadaghiyani et al. [13] developed two new compound type SPTC collector models to determine the efficiency and compared the results with LS-2 and Dudley's model. Stefanovic et al. [14] developed photovoltaic panel integrated hybrid solar collectors to investigate the conversion ability of solar radiation into heat and electricity. Marco et al. [15] investigated the technical difficulties related in utilizing the CuO nanofluid as HTF flowing through transparent quartz receiver. They reached the maximum fluid temperature of 180 °C and an average efficiency of 65%. Visconti et al. [16] designed an electronically operating system to monitor and control two similar solar collectors precisely under the same environment where water and Al_2O_3 nanofluid were used as HTF for exact performance comparison. Colangelo et al. [17] analyzed and compared the thermal efficiency of simulated results with actual experimental results. They proved efficiency enhancement of 7.54% while using Al_2O_3 nanofluid as HTF.

Ghasemi et al. [18] detailed the influence and performance of Al_2O_3/H_2O and CuO/H_2O nanofluid of various concentrations on SPTC. The experimental work was carried out on parabolic trough solar collector to study the thermal and thermophysical properties of Al_2O_3/DI water nanofluid at very low concentration and mass flow rates [19]. Al_2O_3 nanofluid was used as HTF on a SPTC to arrive the techno-commercial analysis of steam power plant [20]. Thomas [21] brought out a straightforward construction and conducted a static load test on collector structure to ensure the stability [21]. The experiment was conducted by Kalogirou [22] on concentrated solar collector as per ASHRAE standard, and they studied the efficiency and incident angle. Thermal performance of therminol on SPTC system was experimentally studied [23]. The performance of SPTC was enhanced with nanofluid concentration and inverse with a mass flow rate of nanofluid [24]. Senthil and Cheralathan carried out experimental works on parabolic dish solar collector's receiver, to analyze the effect of absorber, heat gain and losses. Absorber surface temperature has a positive effect with increased concentration ratio, beam radiation, ambient temperature but opposite sense to air velocity [25]. Impact of thermal energy storage materials in concentrated solar absorbers resulted in improved thermal energy capacity [26].

Farshad and Sheikholeslmi [27] studied the effect of Reynolds number, number of revolutions, diameter ratio, concentration of nanoparticle and wind velocity on exergy loss and heat transfer parameters on flat plate collector, where twisted helical tape and alumina/H_2O nanofluid were used for performance enhancement. Most of the work was carried out in the range of 1.0–5.0% (concentration) and 0.02 kg s^{-1} as the minimum nanofluid flow rate with uneven incremental step in both fluid concentration and mass flow rate.

Based on the above literature, we practiced an attempt to synthesize and analyze Al_2O_3/DI water nanofluid's thermal performance at low concentration (0.2–1.0%) and mass flow rate (0.010 kg s^{-1} and 0.015 kg s^{-1}) at an equal incremental step on unshielded receiver (USR) type SPTC. The significant results are reported in this work.

Fig. 1 Experimental platform of solar collector

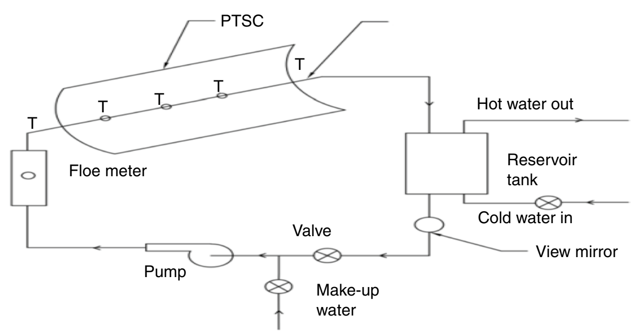

Fig. 2 Schematic diagram of solar collector

Experimental

Construction of SPTC and working procedure

The photographic view of USR type SPTC system for hot water generation test setup and its schematic diagram is shown in Figs. 1 and 2. The test setup consists of SPTC system, heat energy storage tank, nanofluid collection cum recirculation tank, submersible pump, and tracking module. The collector system is included with aperture, receiver, and reflector. The aperture is in the shape of parabolic, where the polished aluminum is fixed, to reflect the solar radiation toward the receiver, which falls on it. The total area of collector aperture or reflector is 1.08 m^2, the length is 1.2 m, and the width is 0.9 m. But the approached effective reflector area is only 1.0593 m^2. The absorber is made of any material (we used copper), but cost, ease of availability, and absorbance capability (varied depends upon the material) must be considered. The copper tube of standard size is used here as an absorber and not shielded by any means. Concentration ratio (ratio of aperture area and absorber area) is a critical parameter that is influencing the useful heat gain. The heat energy collection tank is made up of rigid plastic with proper insulation, to reduce the heat loss. DI water-based alumina nanofluid is selected and utilized as heat transfer fluid due to its extensive experimental reports by researchers, low cost, thermal conductivity, low-pressure drop, low sedimentation and ease of availability.

The USR tube is exposed to reflected radiation coming from the collector aperture, and the heat energy is transferred to HTF. The alumina/DI water nanofluid is heated due to heat transfer from the USR tube by convection mode. The heated alumina/DI water nanofluid is cooled while flows through the heat exchanger where HTF releases the heat energy to hot water by conduction–convection heat exchange mode. A mini submersible pump is used for recirculation and to close the HTF circuit. The experimental work is carried out for two mass flow rates (0.010 kg s^{-1} and 0.0150 kg s^{-1}) controlled by a control valve. The mass flow rates maintain the HTF in the laminar region, up to a certain temperature level. The calculated bulk mean temperature of the fluid is 88 °C and 56 °C for the mass flow rate of

0.010 kg s^{-1} and 0.015 kg s^{-1}, respectively. The bulk mean temperature of HTF is restricted to keep the flowing fluid in the laminar region. SPTE is oriented in the north–south direction, and tracking is carried out in the east–west direction at an angle of 15° automatically for every 1-h time gap, to absorb the maximum radiation. The parametric values are given in Table 1.

Synthesis of nanofluid

The nanofluid is prepared by dissolving the Al_2O_3 nanoparticle (Alfa Aesar) in DI water at five different concentrations from 0.2 to 1.0% v/v. Main properties of alumina nanoparticles are given in Table 2. First, the mass of nanoparticles is calculated using Eq. (1), and then it is mixed with DI water manually and followed by a magnetic stirrer (Remi). Finally, the nanofluid is transferred from magnetic stirrer to ultrasonic bath (Maxsell) for homogeneous mixing. The same procedure is adopted for all concentrations as shown in Fig. 3. The prepared nanofluid has good stability not only due to the two-step preparation procedure, also due to low concentration and mass flow rate.

$$W_{\mathrm{np}} = \left[{}^{V_{\mathrm{np}}}\!/\!{}_{V_{\mathrm{np}} + V_{\mathrm{bf}}} \right] \tag{1}$$

Thermal performance analysis

The instantaneous efficiency of SPTC is determined based on recorded quantities such as solar radiation intensity, ambient temperature, nanofluid inlet temperature, and wind velocity. The absorbed solar radiation depends on the reflectivity of reflector material, and a higher reflectivity leads to higher heat absorption by the fluid as per Eq. (2) [28]. Both the wind loss and radiation loss coefficient are playing a vital role in loss coefficient calculation, which can be determined as per Eq. (3).

Table 1 Specifications of collector system

Parameters	Quantity
Aperture size	1.2 m L × 0.9 m W
Focal length	0.30 m
Receiver diameter	0.0172 m
Reflector material	Polished aluminum
Receiver material	Copper
Orientation	South facing
Concentration ratio	16
Tracking	Single-axis (east–west)
Insulation	Polyurethane
HTF	Al_2O_3/DI water and DI water
Mass flow rate	0.010 kg s^{-1} and 0.015 kg s^{-1}

Table 2 Properties of Al_2O_3 nanoparticles

Properties	Description
Nanoparticle	Aluminum oxide
Shape/form/color	Sphere/powder/white
Particle size, purity	36 nm, 99.5%
Surface area	32–40 m^2 g^{-1}
Density	3.72 g cm^{-3}
Melting/boiling point	2045/2980 °C
Specific heat	765 J kg^{-1} K^{-1}
Thermal conductivity	40 W m^{-1} K^{-1}

Wind loss coefficient is proportional to Nusselt number, and thermal conductivity of air, but inverse to receiver diameter. The radiation loss coefficient depends on the emissivity of receiver material, surface temperature and ambient temperature. The properties such as density, kinematic viscosity, dynamic viscosity, specific heat, Prandtl number, and thermal conductivity were taken from thermo-physical property data. The status of flowing fluid is calculated based on its Reynolds quantity. If the value of $Re < 2300$, then the flow is laminar and coming under fully developed hydrodynamic as well as thermal profile mode. Therefore, $Nu = 3.7$ is considered for constant wall temperature [29]. If the values are in the range of $2300 < Re < 5 \times 10^6$ and $0.5 < Pr < 2000$, then the nanofluid ensures fully developed turbulent flow status. Equations 4 and 5 are represented by Filonienko [30] and Gnielinski [31], used to calculate the friction factor and Nu for turbulent flow, respectively.

$$S = I_b R_b \rho \gamma (\tau\alpha) + I_b R_b (\tau\alpha) \left({}^{D_o}\!/\!{}_{(W + D_o)} \right) \tag{2}$$

Fig. 3 Synthesis of nanofluid

$$U_l = \left[\left({}^{1}/_{h_w}\right) + \left({}^{1}/_{h_r}\right)\right]^{-1} \tag{3}$$

$$f = (1.58 \times \ell n(\mathrm{Re} - 3.28))^{-2} \tag{4}$$

$$\mathrm{Nu} = \frac{\left({}^{f}/_{2}\right)(\mathrm{Re} - 1000)\,\mathrm{Pr}}{1.0 + 12.7\left(\sqrt{{}^{f}/_{2}}\right)\left(\mathrm{Pr}^{2/3} - 1\right)} \tag{5}$$

Due to the absence of variation in the receiver dimension and its thermal conductivity, the heat loss coefficient and inside heat transfer coefficient influenced on overall heat loss coefficient given in Eq. (6). The actual useful heat gain is the difference between useful heat gain and total heat loss which is determined by Eq. (7). The instantaneous collector efficiency is proportional to the actual useful heat gain available as per Eq. (8). Now, the optical efficiency is determined for the various angles of incident by Eq. (9). The optical efficiency (η_{opt}) only depends on the reflectivity (ρ) of aperture material, intercept factor (γ), the transmittance-absorption product of the receiver ($\tau\alpha$). Both the incident angle modifier and end loss were also considered as shown in Eq. (10) to calculate the optical efficiency. The transmittance parameter can be taken 1.0 due to the unshielded type receiver. The inlet–outlet temperature of nanofluid, ambient temperature, and water temperature are observed using the PT-100 resistance temperature detector. The solar power meter, vane-type anemometer, and rotameter are used to measure the beam radiation, wind speed, and mass flow rate. The uncertainty of these measuring instruments is given in Table 3. Each concentration was tested for 3 days. Before charging the next concentration, the existing nanofluid is fully drained. To complete the cleaning process, the test run was conducted with DI water, and then the system is kept in ideal condition. All these parameters are observed at every five minutes.

$$U_o = \left[\left({}^{1}/_{U_l}\right) + \left({}^{D_o}/_{(D_i \times h_{fi})}\right) + \left({}^{D_o}/_{2K_r}\right)\ell n\left({}^{D_o}/_{D_i}\right)\right]^{-1} \tag{6}$$

$$\frac{\partial}{\partial x_j}\left(\rho U_j k\right) - \frac{\partial}{\partial x_j}\left(\frac{\mu_{eff}}{\sigma_k}\frac{\partial U_i}{\partial x_j}\right) = G_{k_1} - \rho\varepsilon \tag{7}$$

$$\eta_{ins} = \left[{}^{Q_u}/_{(I_b R_b W L)}\right] \tag{8}$$

$$\eta_{opt} = (\rho\gamma\tau\alpha) \times K(\theta) \times \left(X_{\text{end loss}}\right) \tag{9}$$

The parametric values measured using the instruments discussed here have not deviated over the limit specified by the ASHRAE standard, which confirms that the experimental works are standard conditions. An uncertainty analysis was carried out based on the procedure suggested by Kline and McClintock [32] and Moffat [33] to validate the experimental measurements. Equation (10) is used to determine the overall uncertainty of the experiment. Equations (10) and (11) are used to determine the overall energy and exergy uncertainty of the experiment.

$$\delta\eta^2 = \left(\frac{\delta\eta}{\delta\dot{m}}\right)^2(\delta\dot{m})^2 + \left(\frac{\delta\eta}{\delta I_b}\right)^2\left(\delta I_b\right)^2 + \left(\frac{\delta\eta}{\delta T_i}\right)^2\left(\delta T_i\right)^2 + \left(\frac{\delta}{\delta T_o}\right)^2\left(\delta T_o\right)^2 \tag{10}$$

$$\left(\delta\eta_{ex}\right)^2 = \left(\frac{\delta\eta_{ex}}{\delta\dot{m}}\right)^2(\delta\dot{m})^2 + +\left(\frac{\delta\eta_{ex}}{\delta I_b}\right)^2\left(\delta I_b\right)^2 + \left(\frac{\delta\eta_{ex}}{\delta T_i}\right)^2\left(\delta T_i\right)^2 + \left(\frac{\delta\eta_{ex}}{\delta T_o}\right)^2\left(\delta T_o\right)^2 + \left(\frac{\delta\eta_{ex}}{\delta T_a}\right)^2\left(\delta T_a\right)^2 \tag{11}$$

Table 3 Uncertainty of measurement

Parameters	Uncertainty/%
Mass flow rate	±1.5
Radiation	±3.5
Temperature	±0.87
Specific heat	±0.10
Collector area	±0.12

By considering the uncertainty of the measuring instruments, while HTF flow rate varied from 0.010 to 0.0150 kg s^{-1}, the experimental energy and exergy uncertainty varied from 5.6 to 4.2% and 3.8 to 2.5%, respectively.

Results and discussion

The results observed from the experimental work are used to analyze the performance of the low volume fraction of alumina/DI water nanofluid on the SPTC with the hot water generation system discussed and presented here.

The variation of ambient temperature and bulk mean temperature for both the mass flow rate of HTF (nanofluid) with respect to the working time of the whole day is given in Fig. 4. There is no abrupt increase in ambient temperature observed for the total module. The ambient temperature starts from 29.0 °C at 8.00 am, and it reaches a maximum of 33.0 °C at 2.00 pm. The difference is only 4.0 °C

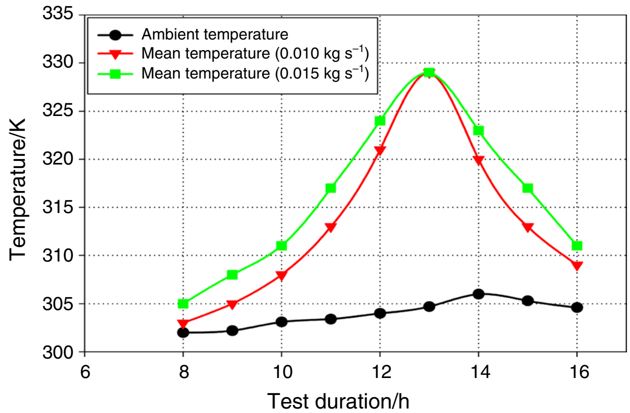

Fig. 4 Variation of T_a and T_m over time

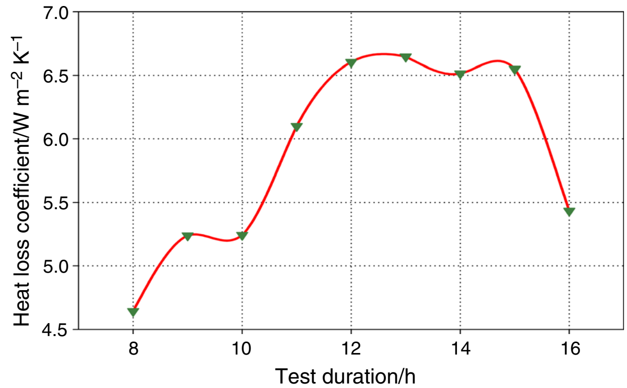

Fig. 6 Heat loss coefficient over time

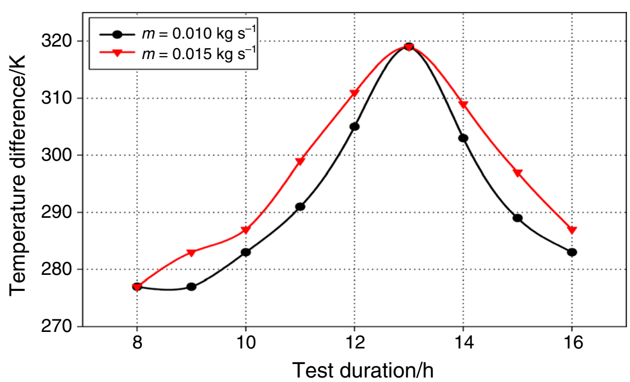

Fig. 5 Temperature rise trend with time

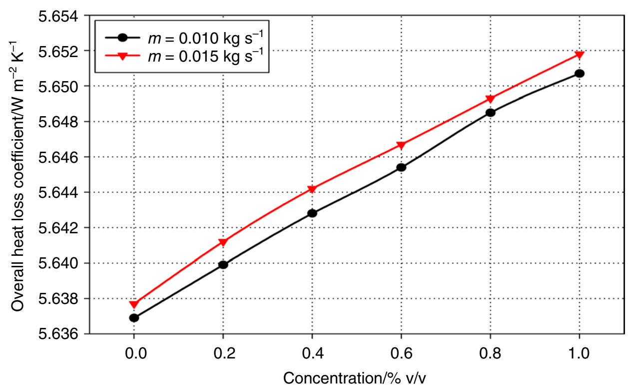

Fig. 7 Overall heat loss coefficient versus concentration

and it depends on the location [23]. At 1.00 pm the bulk mean temperature difference of mass flow rates is zero, before and after this test time it is gradually increased. The bulk mean temperature gradually increases from 30 to 56 °C, and then it is reached to 36 °C. The enhancement of mean temperature is 86.7% for the test duration of 8.00 am to 1.00 pm, and then it is reduced gradually by 55.6%. Variation of the temperature difference between the inlet and outlet for both the mass flow rate of the total test period is given in Fig. 5. The inlet temperature of nanofluid depends not only on the environment but also on the energy absorption capacity of fluid. The fluid outlet temperature depends on the receiver tube temperature and heat transfer coefficient. The receiver temperature is increased by incident solar radiation and the heat transfer coefficient influences outlet temperature. Exactly at 1.00 pm, the temperature difference is equal to both the mass flow rate. The minimum temperature is 4.0 °C, and the maximum difference is 46 °C.

Variation of heat loss coefficient for both the DI water and nanofluid during the test period is shown in Fig. 6. Heat loss is included both wind loss coefficient (h_w) and radiation loss coefficient (h_r). h_w depends on ambient temperature and wind speed. h_r depends on the receiver temperature and emissivity of the receiver. But heat loss coefficient (U_l) is independent of the flowing fluid. Consequently, the observed values apply to both mass flow rates of DI water and nanofluid with various concentrations. U_l is varied from 4.64 to 5.433 W m^{-2} K^{-1} for the whole testing period. At 1.00 pm, the minimum and maximum heat losses are 4.64 W m^{-2} K^{-1}, 6.646 W m^{-2} K^{-1} which is the combined effect of both the loss coefficients. h_r is influenced more and h_w is having a little impact on U_l. Increase in receiver temperature will increase the U_l.

The variation of overall heat loss coefficient (Eq. 5) with the various volume fractions of HTF at defined mass flow rate is given in Fig. 7. The first point, 0% volume fraction means the fluid is only (absence of nanoparticles) DI water. The overall heat loss coefficient is increased with the increase in volume fraction, and it is the combination of heat loss coefficient and inside heat transfer coefficient. The overall loss coefficient for 0.015 kg s^{-1} is more than the mass flow rate of 0.010 kg s^{-1}. It is 5.6369 W m^{-2} K^{-1} and 5.6377 W m^{-2} K^{-1} for water of mass flow rate 0.010 kg s^{-1}

and 0.015 kg s^{-1}. For the concentration of 1.0%, the loss coefficients are 5.6507 W m^{-2} K^{-1} and 5.6518 W m^{-2} K^{-1} corresponding to the given flow rates. The maximum difference for 1.0% volume fraction was meager, i.e. 0.11%. This optical efficiency not varied depends on solar radiation. It belongs and is proportional to the reflective material, absorber material, absorber position, and an incident angle of solar radiation. To obtain the maximum possible optical efficiency, it requires the aperture with high reflectivity, a maximum absorbance-transmittance product and accurate alignment of the receiver. The optical efficiency of the collector has varied from 31.57% in the morning (8.00 am), and it has reached the maximum value (60.75%) in the noon (12.00 pm) again it comes back to the starting point. The overall loss coefficient is high, due to the unshielded receiver and mass flow rate of the liquid. Wind velocity plays a vital role which is considered.

Changes in the quantity of the receiver tube temperature, total available solar radiation (Eq. 6) and the beam radiation with respect to time are given in Fig. 8. The beam radiation is slowly increased, 250 W m^{-2} as a minimum and 850 W m^{-2} as maximum. It depends upon the location of the test setup. The total available solar radiation is also increased proportionally to solar radiation. It depends not only on the solar radiation, but also on the tilt factor and the reflectance of collector material, the intercept factor, absorptive and transmittance of the absorber. Other than the tilt factor, the remaining parameters are influenced more by the total available solar radiation. It performs an influence on the useful heat gain. In the test period of the whole day, the receiver temperature is observed as low in the morning and reached the maximum at noon and near noontime. It is due to the increased quantity of direct solar radiation.

Figure 9 shows the variation of the heat transfer coefficient of the flowing fluid through the absorber with various concentrations. The values are absorbed for the mass flow rate of 0.010 kg s^{-1} and 0.0150 kg s^{-1} with different concentrations. Two opportunities exist to enhance the inside heat transfer coefficient, namely, by increasing the concentration and increasing the mass flow rate. The velocity of the fluid is increased due to mass flow rate; in turn, the inside heat transfer coefficient is increased. An increase in nano-concentration will increase the thermal conductivity of the liquid and heat transfer.

Heat transfer coefficient variation of DI water with time for the mass flow rates are given in Fig. 10. The change in mass flow rate has shown the influence on the heat transfer coefficient. When the mass flow rate is increased, it leads to an increase in heat transfer. The increment is also very gradual from 136.61 to 144.13 W m^{-2} K^{-1}. Here, Nusselt number is constant because flowing fluid is in the laminar region and is equal to 3.7.

Figure 11 shows the inside heat transfer coefficient of the fluid such as DI water (0%) and Al_2O_3/DI water (1.0% volume fraction) nanofluid at the flow rate of 0.01 kg s^{-1} through

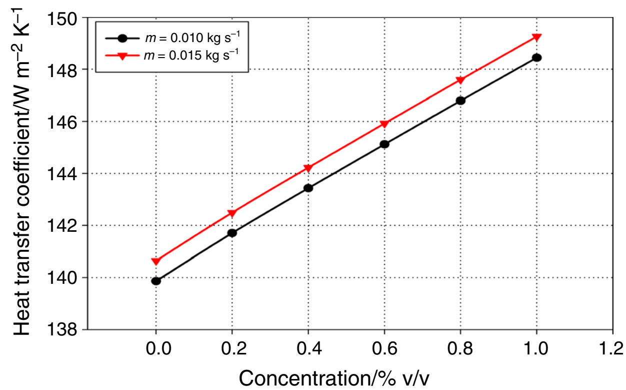

Fig. 9 Variation of heat transfer coefficient with concentration

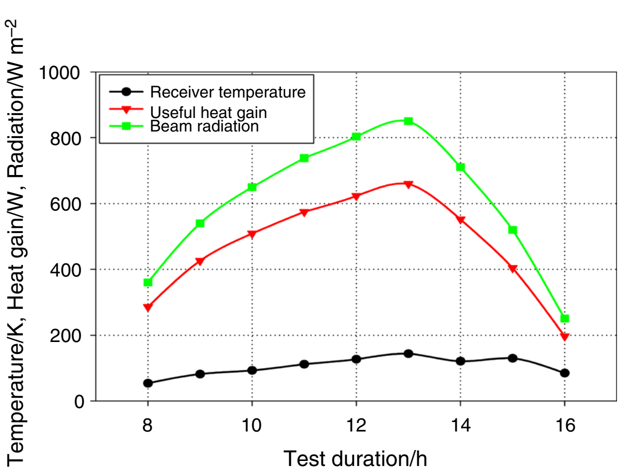

Fig. 8 Variation of receiver temperature, solar flux and beam radiation

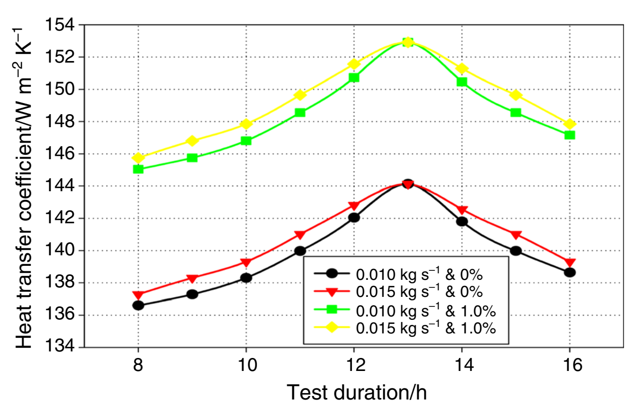

Fig. 10 Heat transfer coefficient over test duration

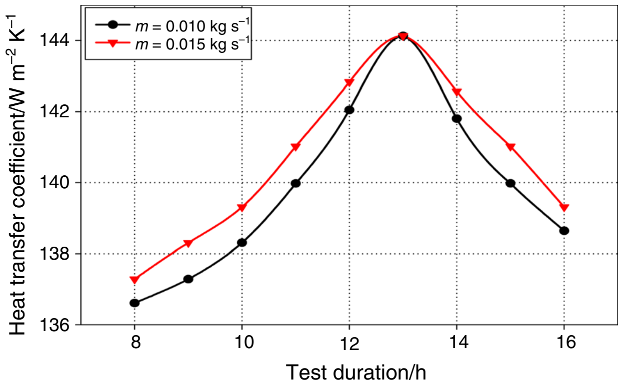

Fig. 11 Comparison of heat transfer coefficient based on flow rate

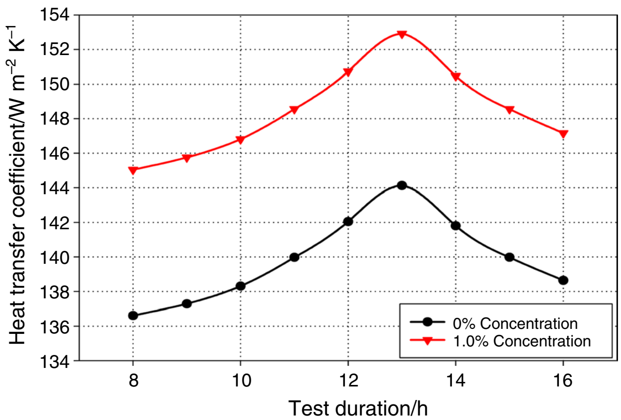

Fig. 12 Comparison of heat transfer coefficient over concentration

the absorber. The same trend is followed for other mass flow rate also. The volume fraction is influenced directly by the heat transfer rate. This heat transfer rate mainly depends on the thermal conductivity of HTF. The heat transfer coefficient is increased from 136.61 to 144.13 W m^{-2} K^{-1} for DI water and 145.04 to 153.00 W m^{-2} K^{-1} for 1.0% volume fraction of nanofluid. The maximum heat transfer rate is 152.91 W m^{-2} K^{-1}. The difference between 0 and 1.0% concentration is 8.8 W m^{-2} K, and the inside heat transfer enhancement is 6.2% as shown in Fig. 12.

The instantaneous collector efficiency for the whole test period from 8.00 am to 4.00 pm is calculated for all volume fractions, and averages of these instantaneous collector efficiencies for each volume fraction are calculated for both the mass flow rates. These efficiency values of nanofluid and

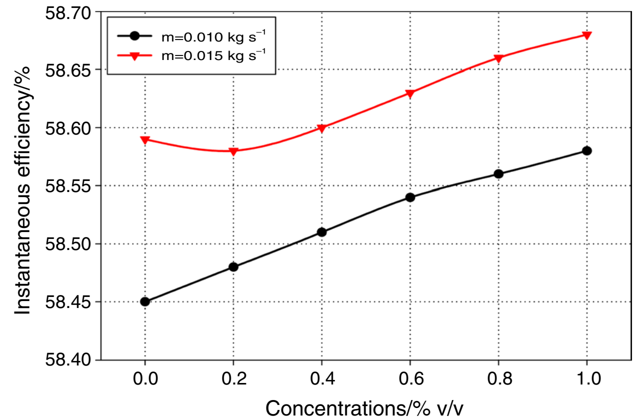

Fig. 13 Comparison of ηth with DI water and Al_2O_3

DI water are presented in Fig. 13. The attained maximum instantaneous efficiency is 59.13% ($m = 0.015$ kg s^{-1}) and 59.05% ($m = 0.010$ kg s^{-1}) for USR copper tube, 55.20% when using water as HTF [34, 35] for the same type receiver. Similar results were attained for alumina-based nanofluid for the mass flow rate of 0.010 kg s^{-1} where alumina and therminol were used as HTF [36, 37]. The reason for this very slight variation in efficiency is glass shielding of copper tube receiver, the diameter of the receiver and mass flow rate of the HTF. The instantaneous collector efficiency is decided by two main factors such as solar radiation and useful heat gain.

The global efficiency equation of the present working model is validated with other researchers as shown in Fig. 14. Here various heat transfer coefficients such as wind loss coefficient, radiation loss coefficient, heat loss coefficient, inside heat transfer coefficient, and overall heat loss coefficient are considered. So, this maximum efficiency point is compared with other efficiency models. The model developed by Marco et al. [15] offered not only maximum energy absorbed but also the quantity of heat loss. The minimum energy was absorbed by Kalogirou et al. model [38]. The absorbed energy is enhanced by 1.51% than Murphy et al. model [39] and 2.95% less than Valanarasu's model [7]. But in the case of removed energy, the present work exhibits lower heat loss than Valanarasu's model [7] and higher than Murphy's model [39]. The current model has good agreement with the previous models developed by Valanarasu and Murphy.

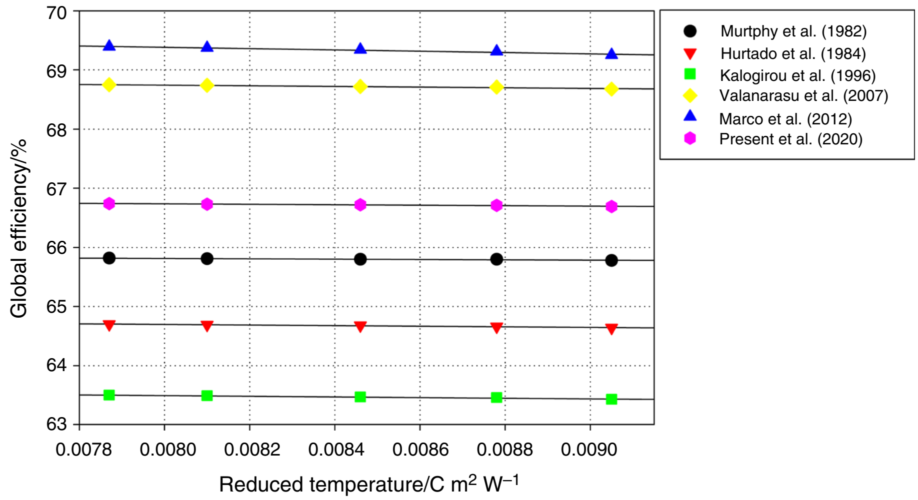

Fig. 14 Performance verification of present model

Conclusions

The thermal performance of alumina/DI water nanofluid at different concentrations and mass flow rates on the concentrated solar concentrator was investigated and compared with DI water. The alumina nanoparticles are mixed with DI water using the magnetic stirrer and then sonicated by an ultrasonic bath for 60 min.

Nanofluid is synthesis at five different concentrations from 0.2 to 1.0% by volume (incremental step 0.2%). The collector efficiency is increased with the increased mass flow rate and concentration of nanoparticles in the base fluid. The increase in the mass flow rate increases thermal efficiency. However, the higher mass flow rate of HTF changes the flow from laminar to turbulent condition.

On an average basis, the maximum collector efficiency for deionized water is 58.45% ($m = 0.010$ kg s^{-1}), 58.59% ($m = 0.015$ kg s^{-1}) and 58.58% ($m = 0.010$ kg s^{-1}), 58.68% ($m = 0.015$ kg s^{-1}) for nanofluid. At the HTF flow rate of 0.010 kg s^{-1} and 0.015 kg s^{-1} mass flow rates, the efficiency enhancements are 1.55% and 1.49% for various nanofluid concentrations.

References

1. Kalogirou SA, Lloyd S. Use of solar parabolic trough collectors for hot water production in Cyprus—a feasibility study. Renew Energy. 1992;12:117–24.
2. Nithyanandam K, Pitchumani R. Optimization of an encapsulated phase change material Thermal energy storage system. Sol Energy. 2014;107:770–88.
3. Sheikholeslami M, Jafaryar M, Shafee A, Babazzadeh H. Acceleration of discharge process of clean energy storage unit with insertion of porous form considering nanoparticle enhanced paraffin. J Clean Prod. 2020;261:121206.
4. Vijayan G, Karunakaran R. Investigation of heat transfer performance of nanofluids on conical solar collector under dynamic condition. Adv Mater Res. 2014;985:1125–31.
5. Vijayan G, Karunakaran R. Experimental investigation on PTSC hot water generation system. J Adv Chem. 2017;13:6054–8.
6. Valanarasu A, Sornakumar SM. Theoretical analysis and experimental verification of parabolic trough solar collector with hot water generation system. Therm Sci. 2007;11(1):119–26.
7. Valanarasu A, Sornakumar SM. Performance characteristics of the solar parabolic trough collector with hot water generation system. Therm Sci. 2006;10(2):167–74.
8. Bellos E, Tzivanidis C, Antonopoulos KA. A detailed working fluid investigation for solar parabolic trough collectors. Appl Therm Eng. 2016;114:374–86.
9. Bellos E, Tzivanidis C. Thermal efficiency enhancement of nanofluid-based parabolic trough collectors. J Therm Anal Calorim. 2019;135(1):597–608.
10. Bellos E, Tzivanidis C. A review of concentrating solar thermal collectors with and without nanofluids. J Therm Anal Calorim. 2019;135(1):763–86.
11. Vijayan G, Karunakaran R. Characteristic analysis of de-ionised water and ethylene glycol based aluminum oxide nanofluid. J Adv Chem. 2017;13(5):6202–7.
12. Murshed SMS, Leong KC, Yang C. Investigations of thermal conductivity and viscosity of nanofluids. Int J Therm Sci. 2008;47:560–8.
13. Sadaghiyani OM, Sadegi A, Khalileria S, Mirzaee I. Two new designs of parabolic solar collectors. Therm Sci. 2014;18(2):323–34.
14. Stefanovic VP, Bojic M. Development and investigation of solar collectors for conversion of solar radiation into heat and/or electricity. Therm Sci. 2006;10(4):177–87.
15. Marco P, Marco M, Gianpiero C, Arturo DR. Experimental investigation of transparent parabolic trough collector based on gas-phase nanofluid. Appl Energy. 2017;203(1):560–70.
16. Visconti P, Primiceri P, Costantini P, Cavalera G. Measurement and control system for thermosolar plant and performance comparison between traditional and nanofluid solar thermal collectors. Int J Smart Sens Intell Syst. 2016;9(3):681–708.
17. Colangelo G, Milanese M, Risi AD. Numerical simulation of thermal efficiency of an innovative Al_2O_3 nanofluid solar thermal collector: influence of nanoparticles concentration. Therm Sci. 2017;21(6B):2769–79.

18. Ghasemi SE, Ranjbar AA. Effect of nanoparticles in working fluid on thermal performance of solar parabolic trough collector. J Mol Liq. 2016;222:159–66.
19. Subramani J, Nagarajan PK, Wongwises S, El-Agouz SA, Sathyamurthy R. Experimental study on the thermal performance and heat transfer characteristics of solar parabolic trough collector using Al_2O_3 nanofluids. Environ Prog Sustain Energy. 2018;37:1149–59.
20. Khan MS, Abid M, Ratlamwala TAH. Energy, exergy and economic feasibility analyses of a 60 MW conventional steam power plant integrated with parabolic trough solar collectors using nanofluids. Iran J Sci Technol Trans Mech Eng 2017;1–17.
21. Thomas A. Simple structure for parabolic trough concentrator. Energy Convers Manag. 1994;35:569–73.
22. Kalogirou SA. Parabolic trough collector system for low-temperature steam generation: design and performance characteristics. Appl Energy. 1996;55:1–19.
23. Kumaresan G, Rahulram S, Velraj R. Performance studies of a solar parabolic trough collector with a thermal energy storage system. Energy. 2012;47:395–402.
24. Vijayan G, Karunakaran R. Performance evaluation of nanofluid on parabolic trough solar collector. Therm Sci. 2020;24(2A):853–64.
25. Senthil R, Cheralathan M. Effect of non-uniform temperature distribution on surface absorption receiver in parabolic dish solar concentrator. Therm Sci. 2017;21(4):2011–9.
26. Senthil R, Cheralathan M. Enhancement of the thermal energy storage capacity of a parabolic dish concentrated solar receiver using phase change materials. J Energy Storage. 2019;25:100841.
27. Farshad SA, Sheikholeslami M. Nanofluid flow inside a solar collector utilizing twisted tape considering exergy and entropy analysis. Renew Energy. 2019;141:246–58.
28. Duffie JA, Beckman WA. Solar engineering of thermal processes. New York: John Wiley and Sons; 1991.
29. Brooks MJ, Mills I, Harms TM. Performance of a parabolic trough solar collector. J Energy South Afr. 2006;17(3):71–80.
30. Filonienko GK. Friction factor for turbulent pipe flow. Teploenergetika. 1954;1(4):40–4.
31. Gnielinski V. New equations for heat and mass transfer in the turbulent pipe and channel flow. Int J Chem Eng. 1976;16:359–68.
32. Kline S, McClintock F. Describing uncertainties in single-sample experiments. Mech Eng. 1953;75:3–8.
33. Moffat RJ. Describing the uncertainties in experimental results. Exp Therm Fluid Sci. 1988;1:3–17.
34. Senthil R. Thermal performance of aluminum oxide based nanofluids in flat plate solar collector. Int J Eng Adv Technol. 2019;8(3):445–8.
35. Khullar V, Tyagi H. Application of nanofluids as the working fluid in concentrating parabolic solar collectors. In: Proceedings of international conference on fluid mechanics and Fluid power. IIT Madras, Chennai, 2010; 1–9.
36. Singh H. Singh PA review paper on performance improvement of parabolic trough collector system. J Appl Mech Eng. 2015;4(2):1–10.
37. Rasih RA, Sidik NAC, Samion S. Recent progress on concentrating direct absorption solar collector using nanofluids: a review. J Therm Anal Calorim. 2019;137(3):903–22.
38. Kalogirou S. Parabolic trough collector system for low temperature steam generation: design and performance characteristics. Appl Energy. 1996;55(1):1–19.
39. Murphy LM., Keneth E. Steam generation in line-focus solar collectors: A comparative assessment of thermal performance, operating stability, and cost issues. In: SERI/TR-1311; 1982. https://doi.org/10.2172/5247106.